THE JOURNAL OF PHYSICAL CHEMISTRY C LETTERS

2007, *111,* 18451−18456
Published on Web 11/23/2007

ZnO−TiO_2 Core−Shell Nanorod/P3HT Solar Cells

Lori E. Greene, Matt Law, Benjamin D. Yuhas, and Peidong Yang*

Department of Chemistry, University of California, Berkeley, Berkeley, California 94720, and Materials Sciences Division, Lawrence Berkeley National Laboratory, 1 Cyclotron Road, Berkeley, California 94705

Received: September 20, 2007; In Final Form: November 6, 2007

We evaluate an ordered organic−inorganic solar cell architecture based on ZnO−TiO_2 core−shell nanorod arrays encased in the hole-conducting polymer P3HT. Thin shells of TiO_2 grown on the ZnO nanorods by atomic layer deposition significantly increase the voltage and fill factor relative to devices without shells. We find that the core−shell cells must be exposed to air to reproducibly attain efficiencies higher than 0.05%. Cells stored in air for 1 month are 0.29% efficient.

Introduction

Donor−acceptor solar cells convert sunlight to electrical power by splitting photogenerated excitons across an interface between an electron donor and an electron acceptor material.[1] The external quantum efficiency of a solar cell based on exciton dissociation at a donor−acceptor interface is $\eta_{EQE} = \eta_A(\lambda) \times \eta_{ED} \times \eta_{CC}$, where $\eta_A(\lambda)$ is the photon absorption efficiency, η_{ED} is the fraction of excitons that dissociate into free carriers at a donor−acceptor site before recombining, and η_{CC} is the fraction of carriers collected at the device electrodes. In cells with planar junctions, the power conversion efficiency is limited because the exciton diffusion length of the donor material is typically significantly shorter than its absorption length, resulting in a low η_{ED}. This problem, known as the exciton diffusion bottleneck, has been addressed in organic and organic−inorganic hybrid solar cells by adopting a bulk heterojunction topology, in which the donor and acceptor phases are intimately mixed such that the majority of excitons are generated within a diffusion length of the interface.[2,3] Complete quenching of the photoluminescence in bulk heterojunction devices suggests that η_{ED} can be near unity, resulting in NREL-certified device efficiencies above 5% for state-of-the-art cells based on poly(3-hexyl)thiophene (P3HT) and [6]-phenyl C_{61} butyric acid methyl ester (PCBM).[4] The respectable efficiencies of certain bulk heterojunction cells may soon enable the marketing of these devices as low-cost alternatives to conventional thin-film photovoltaics.

Polymer−inorganic hybrid solar cells are of particular interest because they combine the solution processability of polymers with the high electron mobility of inorganic semiconductors.[5] Hole-conducting polymers have been combined with a wide range of inorganic nanomaterials, including CdSe quantum dots, rods, tetrapods and hyper-branched colloids,[6−9] TiO_2 and ZnO nanocrystals,[5,10−17] and PbS, PbSe, $CuInS_2$, and $CuInSe_2$ nanoparticles.[18−22] The active layers of these devices are formed by phase separation during the spin coating of mixtures of the polymer and inorganic material. Spin coating typically produces an isotropic dispersion of the two phases in which the topology is dictated by the interplay of surface energies and the kinetics of solvent evaporation. Charge transport in isotropic bulk heterojunctions can be inefficient because the disordered, interpenetrating networks of the two phases result in tortuous conduction pathways, low carrier mobilities and trapped charge in isolated phase pockets and cul-de-sacs. In many cases, the switch to a bulk heterojunction has replaced the exciton diffusion bottleneck with a charge transport bottleneck.[23,24]

The perceived charge transport limitations of isotropic bulk heterojunctions have prompted attempts to create ordered film architectures.[8,25−27] Several theoretical studies conclude that the ideal polymer-inorganic device topology is a perfect vertical array of single-crystalline nanorods of the appropriate dimensions and pitch, encased in a film of the polymer.[28,29] The nanorods should complement the polymer as a light absorber in addition to serving as the electron acceptor. In principle, the nanorod design is optimal because it (i) provides direct channels for electron and hole transport to the electrodes, (ii) features a higher electron mobility in the inorganic phase, and (iii) provides a scaffold on which the polymer can be annealed to optimize its hole mobility without the risk of phase separation. Over the past several years, we have developed ZnO nanorod arrays suitable for both polymer-inorganic cells and dye-sensitized cells.[30−33] Several groups have built polymer-inorganic cells from their own ZnO rod arrays, but in general the devices perform poorly. For instance, NREL researchers reported a P3HT/ZnO rod cell exhibiting a short-circuit current density (J_{SC}) of 2.2 mA/cm^2, an open-circuit voltage (V_{OC}) of 0.44 V, a fill factor (FF) of 0.56, and an efficiency of 0.53% using nanorods grown in basic conditions.[34] Soon afterward, Ravirajan et al.[35] and Peiro et al.[36] used several types of hydrothermally grown ZnO rod arrays with P3HT but achieved a lower efficiency of 0.2% only after coating the nanorods with an amphiphilic dye prior to P3HT deposition. Efforts create ordered P3HT/TiO_2 cells by filling P3HT into the regular channels of mesoporous TiO_2 films have been foiled by the poor filling and crystallinity of the P3HT within the narrow mesopores.[37,38] At present, the best isotropic polymer−metal oxide bulk hetero-

* Corresponding author. E-mail: p_yang@berkeley.edu.

10.1021/jp077593l CCC: $37.00

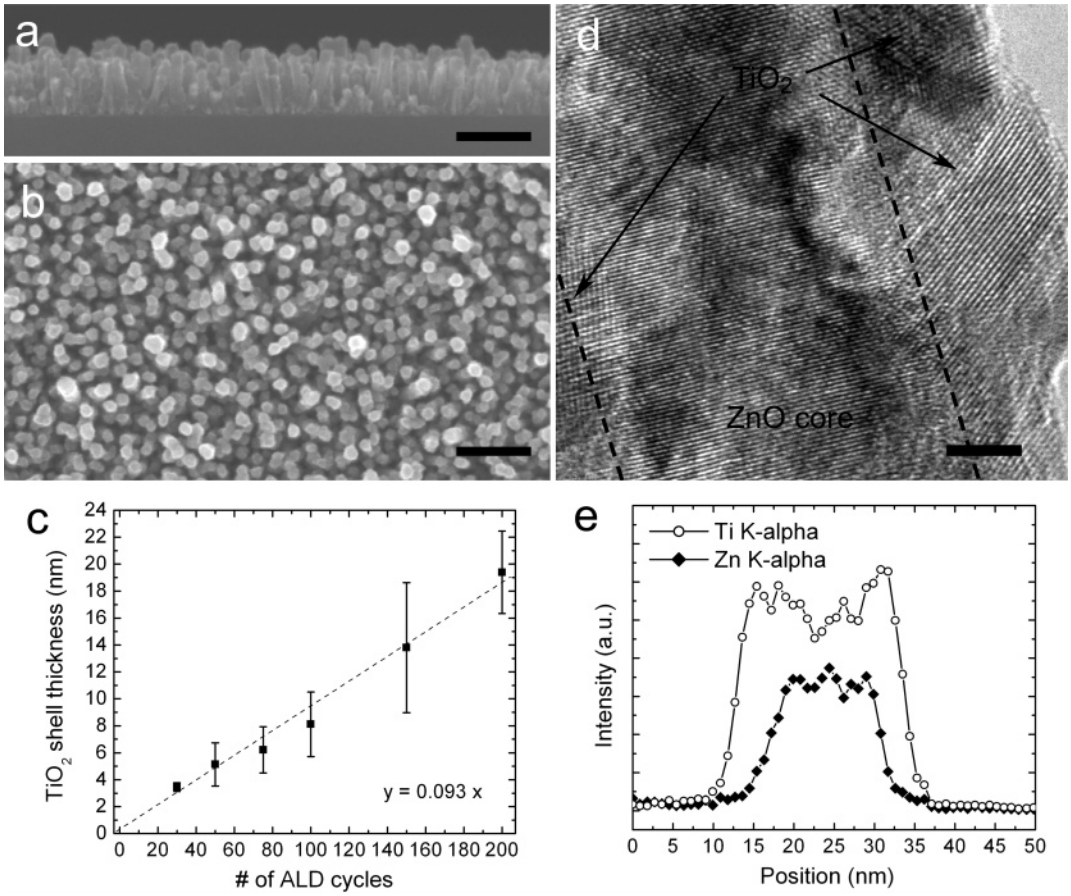

Figure 1. Structural characterization of the ZnO−TiO_2 core−shell nanorod arrays used in this study. (a) Cross-sectional and (b) plan-view SEM images of a ZnO nanorod array on silicon coated with 6 nm of TiO_2 by ALD. Scale bars, 200 nm. (c) TiO_2 shell thickness against number of ALD cycles. Error bars represent one standard deviation of 30 data points. The dashed line is a least-squares fit, intercept set at origin. (d) High-resolution TEM image of a ZnO−TiO_2 nanorod, showing a single-crystalline ZnO core coated with polycrystalline anatase TiO_2 (as determined by XRD (not shown)). Scale bar, 5 nm. The ZnO core is outlined with dashed lines. (e) Corresponding energy dispersive spectroscopy (EDS) elemental linescan across the nanorod.

junctions outperform the ordered architectures by a factor of 2−3.[5,10,11,15,39]

Here we show that the efficiency of our P3HT/ZnO nanorod solar cells can be improved 5-fold by coating the nanorod arrays in a thin shell of TiO_2 using atomic layer deposition (ALD). We find that cells built from uncoated ZnO rod arrays synthesized by the zinc nitrate and hexamethylenetetramine route are barely functional. Suspecting that the ZnO/P3HT interface is not a suitable one for charge separation, we replaced it with a TiO_2/P3HT interface, which is known to readily split excitons generated in P3HT.[29] Although bulk ZnO and TiO_2 have similar band gaps (∼3.2 eV) and band edge energies,[40] they can have very different surface chemistry, doping, and resistivity.[40−45] For example, previous measurements yielded a resistivity of ∼1 Ω cm for our ZnO nanowires[32] and 10^3−10^4 Ω cm for TiO_2 films made by ALD.[46] As a result, the interfacial structure and charge-transfer dynamics of TiO_2/P3HT and ZnO/P3HT interfaces could be quite different. Coating the ZnO nanorod arrays with titania shells 4−10 nm in thickness causes a dramatic increase in V_{OC} and fill factor, possibly by increasing the efficiency of exciton dissociation across the organic−metal oxide interface and/or acting as an energy barrier to retard recombination. The performance of the core−shell devices depends critically on exposure to air, with the best devices showing efficiencies of 0.29% under 100 mW/cm^2 AM 1.5 irradiance after 1 month of storage in air.

Materials and Methods

Nanorod Array Synthesis. ZnO nanorod arrays were made in a two-step aqueous process identical to our previously published method.[31] Indium tin oxide (ITO) substrates (20 Ω/square, Thin Film Devices, Inc.) were sonicated in acetone/ethanol, 1 M HCl and again in pure ethanol, then rinsed in ethanol and dried in a stream of nitrogen. Textured ZnO nanocrystal seeds were formed on the substrates by coating them with a drop of 0.005 M zinc acetate dihydrate (98%, Aldrich) in ethanol, rinsing with ethanol just before the droplet dries, and then heating the ITO at 350 °C in air for 20 min. Vertical nanorod arrays were grown by immersing the seeded substrates in unstirred aqueous solutions of 25 mM zinc nitrate hexahydrate, 25 mM hexamethylenetetramine, and 5−7 mM polyethylenimine for 30 min at 80 °C, producing nanorods with an average size of 20 × 200 nm. To reduce the density of free-floating ZnO particulates capable of short-circuiting our devices, each solution was maintained at 95 °C for 1 h before the substrates were introduced at 80 °C.

TiO_2 shells were grown on the arrays in a homemade traveling-wave ALD system using $TiCl_4$ (99.999%, Alfa) and water at 300 °C with a process pressure of 300−500 mTorr, yielding an average growth rate of 0.9 Å per cycle.

Device Fabrication. A portion of each nanorod array was removed with a swab soaked in 1 M HCl to produce a clean area for electrical contact to ITO. The substrates were then rinsed thoroughly with water, blown dry in nitrogen, heated to 200 °C

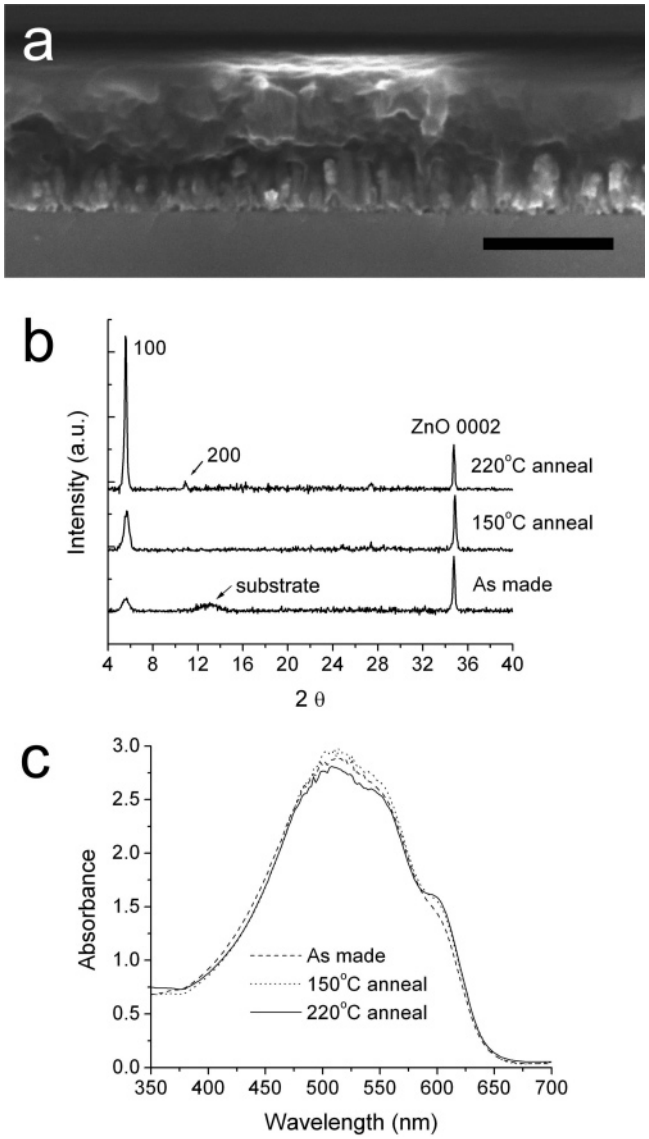

Figure 2. Characterization of the P3HT/core−shell nanorod composite film. (a) Cross-sectional SEM image of a ZnO−TiO_2 array grown on silicon and then infiltrated with P3HT (30 mg/mL P3HT in chloroform spun at 600 rpm and annealed at 220 °C for 1 h). Scale bar, 200 nm. (b) XRD patterns and (c) absorption spectra of P3HT/nanorod films on glass as a function of annealing treatment.

in air for 10 min and, while still warm, transferred into an argon glove box. 100 μL of a 30 mg/mL solution of regioregular, electronic-grade P3HT (Rieke Metals Inc., USA) in chloroform was then spin cast onto the nanorod film at 600 rpm, resulting in 600 nm thick films. The films were annealed in the glovebox at 220 °C for 1 h to improve P3HT infiltration and crystallinity. Gold electrodes (100 nm thick) were deposited at a pressure of $<10^{-6}$ Torr in a thermal evaporator within the same glovebox to create eight distinct 0.03 cm^2 devices on each substrate. The ITO contact region was exposed by removing the overlying P3HT with a swab soaked in $CHCl_3$ and coated with silver paste to guarantee good contact to the pins of the measurement cell. The devices were tested in either argon or air under AM 1.5G simulated sunlight (300 W Model 91160, Oriel). External quantum efficiency (EQE) values (uncorrected for transmission and reflection losses) were obtained with a 150 W xenon lamp coupled to a monochromator and calibrated with a silicon photodiode.

Air Treatments. The samples were wrapped in aluminum foil, transferred to air and either annealed in the dark at 120 °C for 2 h or stored in air in a dark drawer for an allotted time. Air-exposed samples were tested in air.

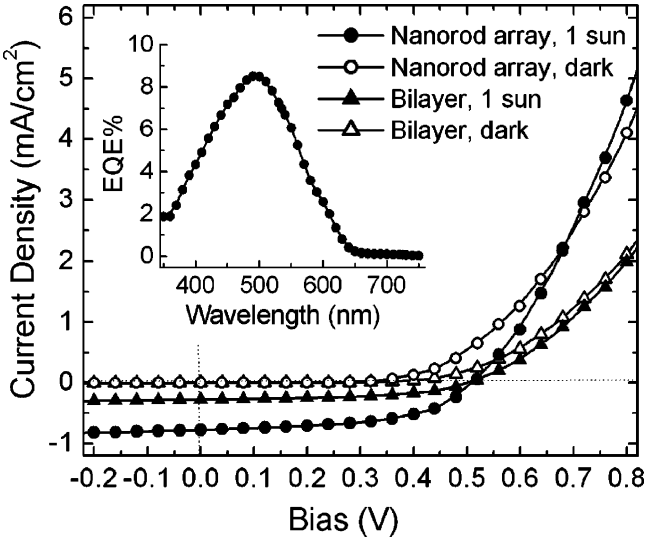

Figure 3. $J-V$ plots of a ZnO−TiO_2 nanorod/P3HT cell with a 7 nm shell (circles) and a P3HT/TiO_2 bilayer cell (triangles) in the dark (open symbols) and under 100 mW cm^{-2} AM 1.5 simulated illumination (closed symbols). The inset is the external quantum efficiency of the nanorod cell.

Structural Characterization. Transmission electron microscopy (TEM) was performed on a Philips CM200/FEG TEM operating at 200 kV, and an FEI Strata 235 was used for scanning electron microscopy (SEM) imaging. X-ray diffraction (XRD) data were obtained on a Siemens D500 diffractometer (Cu Kα radiation) and optical absorption spectra were acquired with an Agilent 8453 UV−vis spectrophotometer.

Results and Discussion

Figure 1 presents basic electron microscopy characterization of ZnO−TiO_2 core−shell nanorods with 6 nm thick shells. The uncoated ZnO rods are 150−225 nm long and 15−25 nm in diameter, stand vertical to within 5−10° of the substrate normal and have a pitch of 45 ± 13 nm. TEM measurements of individual core−shell rods determined that the TiO_2 shell thickness increases at a rate of 0.9 Å per ALD cycle (Figure 1c). Shells thinner than 4 nm are conformal, amorphous, and smooth, and thicker shells are polycrystalline anatase and, due to variations in grain size, fairly rough. The crystalline grains seem to nucleate from the ZnO/TiO_2 interface, with individual grains eventually spanning the entire shell thickness. The shells are fully crystalline when thicker than 9−10 nm.

Characterization of P3HT-filled core−shell rod films with a shell thickness of 7 nm and total film thickness of 600 nm is presented in Figure 2. SEM images of films annealed at 220 °C, around the melting point of P3HT,[47] suggest that the polymer completely fills the nanorod array. XRD and optical absorption data show that annealing the composite film substantially improves the P3HT crystallinity, which should enhance its hole mobility.[48−50] Increasing the annealing temperature from 150 to 220 °C intensifies and sharpens the P3HT 100 diffraction peak, which originates from crystals with their alkyl chains oriented perpendicular and their $\pi-\pi$ stacking axis parallel to the substrate surface.[49,51] XRD of composite films with a minimal P3HT overlayer gave similar results, indicating that P3HT crystallization readily occurs within the interstices of the nanorod array. Absorption spectra of composite films show the development of a well-defined shoulder at 603 nm upon

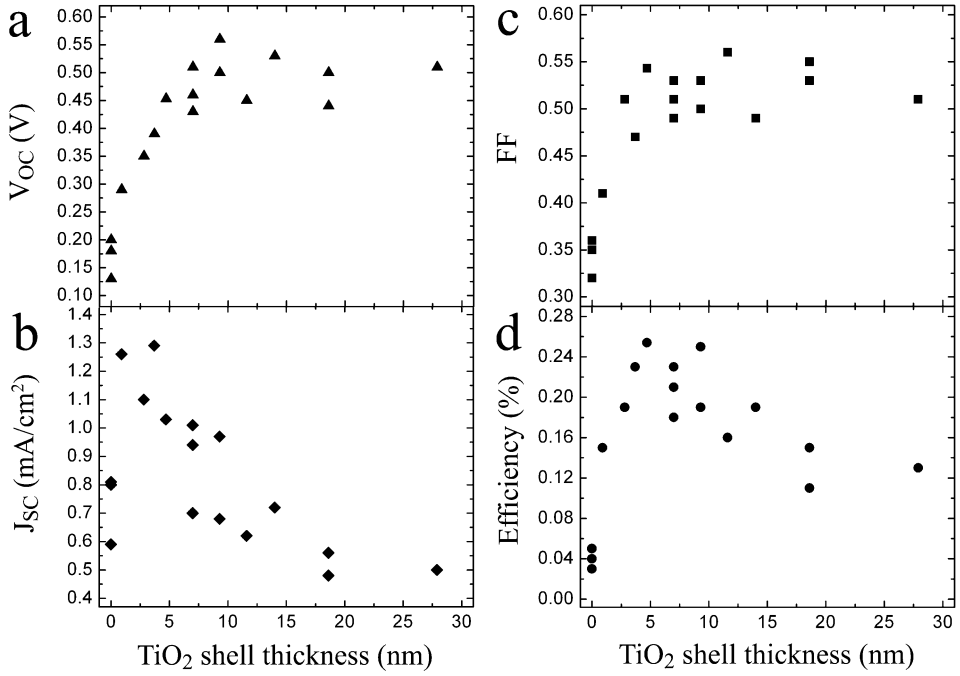

Figure 4. Trends in the performance parameters of the core−shell cells as a function of TiO_2 shell thickness: (a) V_{OC}; (b) J_{SC}; (c) FF; (d) efficiency. Each data point is an average of four devices.

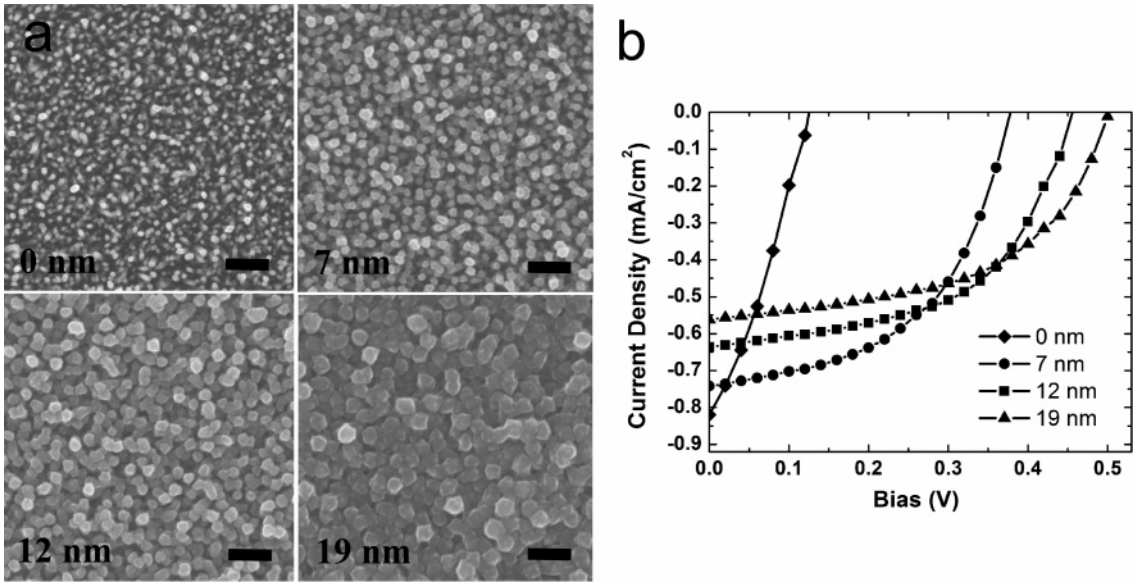

Figure 5. TiO_2 shell thickness and device performance. a) Plan-view SEM images of ZnO nanorod arrays with TiO_2 shells of different thickness. Scale bars, 200 nm. (b) Corresponding $J-V$ plots. The devices were annealed in air at 120 °C for 2 h. Plots are an average of seven devices.

annealing. This feature is associated with an increase in molecular order in P3HT films.[52,53]

We first describe the performance of core−shell devices with 7 nm shells. After deposition of the top contact, the devices were annealed in air in the dark at 120 °C for 2 h and then tested in air. The current density−voltage ($J-V$) plot of a typical device is characterized by $J_{SC} = 0.77$ mA/cm^2, $V_{OC} = 0.51$ V, FF = 0.54, and an efficiency of 0.23% (Figure 3). The external quantum efficiency (EQE) of this cell peaks at 8.5% near the absorption maximum of P3HT (495 nm). Because these 600 nm thick films absorb >90% of the light from 425−625 nm, the EQE must be limited by exciton dissociation and carrier recombination. Identical devices made with 100 nm thick P3HT overlayers showed similar J_{SC} values, suggesting that poor exciton splitting rather than charge transport limits the efficiency. This hypothesis is supported by comparing the core−shell nanorod cells with P3HT/TiO_2 bilayer cells prepared identically except without a ZnO rod array (Figure 3). The nanorod devices show currents three times larger than the bilayer devices, indicating that the increased interfacial area due to the rods improves η_{ED}.

We find that both a ZnO−TiO_2 core−shell geometry and air exposure are required to produce cells with efficiencies reproducibly higher than 0.05%. In other words, neither air-annealed ZnO nanorod cells without shells nor core−shell cells protected from air work well. Nanorod cells without shells or air exposure show quasi-linear $I-V$ curves and no photovoltaic effect, in agreement with Peiro et al.[36] Upon air exposure, our bare nanorod cells become rectifying but never more than 0.05% efficient (see Figure S1 and Figure 5). Soon after the submission of this manuscript, Olson et al.[54] reported a 0.28% efficient, air-annealed ZnO nanorod/P3HT device using a similar rod

synthesis but without PEI. These authors employ silver top contacts, shorter polymer annealing times and dichlorobenzene as the P3HT solvent. Because these devices are annealed at the melting point of P3HT, the P3HT crystallinity and morphology should not depend on the casting solvent. We also noticed no difference in our results between silver and gold top contacts. At present, we cannot account for this difference in device efficiency.

To better understand the function of the oxide shell, we tested several additional cell structures that featured ALD-grown ZnO layers. All devices were air exposed. Core−shell cells made with ALD-deposited ZnO shells (25 nm thick) showed similar rectification behavior but smaller currents than the uncoated ZnO rod cells, as did P3HT/ZnO bilayer devices using 80 nm thick ZnO thin films. Both devices are essentially bilayer devices, with the decreased currents caused by a smaller interfacial area. Furthermore, cells made from ZnO rods grown from ITO substrates coated with 25 nm ALD-deposited ZnO thin films had efficiencies similar to those of the uncoated ZnO rod cells. Finally, trilayer cells made from ITO substrates coated with 25 nm of ALD-deposited ZnO and 5 nm of ALD-deposited TiO_2 worked like typical P3HT/TiO_2 bilayer devices. These experiments illustrate the key role played by the TiO_2/P3HT (and perhaps the TiO_2/ZnO) interface in our devices.

Figure 4 shows the dependence of J_{SC}, V_{OC}, FF, and efficiency on TiO_2 shell thickness for a series of devices annealed in air in the dark at 120 °C for 2 h and tested in air. Control ZnO nanorod cells without shells were held at 300 °C and 300 mTorr for 1 h to mimic the conditions experienced by the core−shell cells. Devices without shells had the following average characteristics: $J_{SC} = 0.74$ mA/cm^2, $V_{OC} = 0.17$ V, FF = 0.34, and an efficiency of 0.04%. Both the open-circuit voltage and fill factor increase rapidly with TiO_2 thickness and plateau at 0.5−0.55 V and 0.5−0.56, respectively, at a shell thickness of 5−10 nm. Meanwhile, the short-circuit current initially doubles to over 1 mA/cm^2 with thin (<5 nm), amorphous shells, then decreases quasi-linearly with thicker shells. We believe that the J_{SC} falls because the thickening shells progressively reduce the volume within the nanorod array available to the polymer. Eventually, the nanorods coalesce to form a thin film at a shell thickness of about 20 nm (Figure 5). Devices made from these coalesced arrays show J_{SC} values very similar to those of our bilayer devices (see Figure 3). The overall efficiency of the core−shell cells peaks at 0.25% at an optimal TiO_2 thickness of 5−9 nm.

The impact of air exposure on core−shell device performance is illustrated in Figure 6. Here, cells with 7 nm shells were exposed to laboratory air in the dark at room temperature for a specified period of time, then tested in air. Air exposure is found to positively affect J_{SC}, V_{OC}, and FF. One day in the air increases cell efficiency from 0.03% to 0.18%. Additional time in air augments J_{SC} and FF, with devices stored for 1 month yielding the following average performance, our best to date: $J_{SC} = 1.14$ mA/cm^2, $V_{OC} = 0.50$ V, FF = 0.50, and an efficiency of 0.29%. We cannot rule out the possibility of alternative air treatments giving higher efficiencies.

The beneficial, often crucial, effect of air on P3HT/ZnO and P3HT/TiO_2 solar cells has been reported by others.[5,34,55−57] A leading explanation for this behavior comes from studies showing that metal oxide thin films spontaneously lose surface oxygen when in vacuum (as during evaporation of the top electrode), oxygen-free ambient or in contact with certain polymers.[58−61] Loss of oxygen renders the oxide surface electron rich and, it is claimed, converts the oxide into an electron donor,

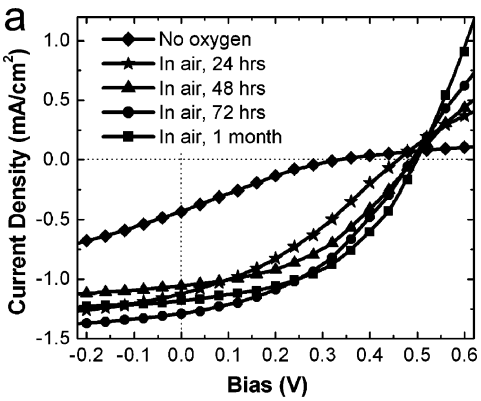

b

	No oxygen	In air, 24 hrs	In air, 48 hrs	In air, 72 hrs	In air, 1 month
V_{OC}	0.34	0.46	0.50	0.48	0.50
J_{SC}	0.45	1.07	0.99	1.24	1.14
FF	0.23	0.37	0.45	0.45	0.50
η	**0.03**	**0.18**	**0.23**	**0.27**	**0.29**

Figure 6. Effect of air exposure on core−shell cell performance. Devices with 7 nm thick shells were exposed to air in the dark for times ranging from 24 h to 1 month. (a) $J-V$ plots. (b) Performance parameters. Devices exposed to air for 48 h showed similar performance to devices annealed in air at 120 °C for 2 h. Plots are averages of four devices.

disrupting device function.[56,57] Isotope methods were used to show that, upon exposing polymer/Nb_2O_5 bilayer devices to oxygen gas, oxygen is reabsorbed at the Nb_2O_5 surface and device performance improves.[57] If facile oxygen loss is a general phenomenon in such devices, the opposing positive effect of oxygen on oxide stability and negative effect of oxygen on polymer stability bode ill for the future of metal oxide−polymer solar cells.

Conclusions

We have shown that coating vertical ZnO nanorod arrays with 4−10 nm of TiO_2 improves the efficiency of our nanorod/P3HT solar cells 5-fold. The TiO_2 shell causes a large increase in V_{OC} and fill factor, resulting in an efficiency of 0.29% for devices stored in air for 1 month. We propose two reasons why these nanorod cells do not have a higher efficiency. The first is chemical: our ZnO nanorods do not readily form a good charge separation interface with P3HT and show poor performance even after exposure to air. The second reason for the disappointing performance of these cells is structural: the nonabsorbing nanorod arrays are too densely packed, especially after adding the TiO_2 shells, making for an insufficient polymer filling fraction and low $\eta_A \times \eta_{ED}$. It remains an open challenge to synthesize an ordered inorganic scaffold with the correct dimensions to enable the fabrication of a highly efficient polymer-inorganic solar cell, mostly because of the short exciton diffusion lengths of popular polymers and the difficulty of making nanorod arrays of semiconductors that have an optimal band gap. To achieve a high efficiency nanorod-polymer solar cell, it is important to optimize both the band gap of the high-density nanorod material and the organic−inorganic interface for effective charge separation.

Acknowledgment. We thank N. Fromer, K. Sivula, C. Wadia, and I. Gur for discussions, and A. P. Alivisatos for use of the solar simulator and glove box. We thank the National Center for Electron Microscopy, Lawrence Berkeley National Laboratory, Berkeley, for the use of their facilities. This work

was supported by the U.S. Department of Energy, Office of Basic Sciences. L.G. was partially supported by a Berkeley-ITRI fellowship.

Supporting Information Available: *J*−*V* plots comparing a ZnO nanorod/P3HT cell and ZnO−TiO_2 nanorod/P3HT cell with a 7 nm shell in the dark and under illumination. This material is available free of charge via the Internet at http://pubs.acs.org.

References and Notes

(1) Nelson, J. *Curr. Opini. Solid State Mater. Sci.* **2002**, *6*, 87−95.
(2) Peumans, P.; Uchida, S.; Forrest, S. R. *Nature* **2003**, *425*, 158−162.
(3) Yu, G.; Gao, J.; Hummelen, J. C.; Wudl, F.; Heeger, A. J. *Science* **1995**, *270*, 1789−1791.
(4) Kim, J. Y.; Kim, S. H.; Lee, H. H.; Lee, K.; Ma, W. L.; Gong, X.; Heeger, A. J. *Adv. Mater.* **2006**, *18*, 572.
(5) Beek, W. J. E.; Wienk, M. M.; Janssen, R. A. J. *Adv. Funct. Mater.* **2006**, *16*, 1112−1116.
(6) Sun, B. Q.; Greenham, N. C. *Phys. Chem. Chem. Phys.* **2006**, *8*, 3557−3560.
(7) Huynh, W. U.; Dittmer, J. J.; Alivisatos, A. P. *Science* **2002**, *295*, 2425−2427.
(8) Gur, I.; Fromer, N. A.; Chen, C. P.; Kanaras, A. G.; Alivisatos, A. P. *Nano Lett.* **2007**, *7*, 409−414.
(9) Sun, B. Q.; Marx, E.; Greenham, N. C. *Nano Lett.* **2003**, *3*, 961−963.
(10) Kwong, C. Y.; Choy, W. C. H.; Djurisic, A. B.; Chui, P. C.; Cheng, K. W.; Chan, W. K. *Nanotechnology* **2004**, *15*, 1156−1161.
(11) Zeng, T. W.; Lin, Y. Y.; Lo, H. H.; Chen, C. W.; Chen, C. H.; Liou, S. C.; Huang, H. Y.; Su, W. F. *Nanotechnology* **2006**, *17*, 5387−5392.
(12) Slooff, L. H.; Wienk, M. M.; Kroon, J. M. *Thin Solid Films* **2004**, *451*−*52*, 634−638.
(13) van Hal, P. A.; Wienk, M. M.; Kroon, J. M.; Verhees, W. J. H.; Slooff, L. H.; van Gennip, W. J. H.; Jonkheijm, P.; Janssen, R. A. J. *Adv. Mater.* **2003**, *15*, 118.
(14) Arango, A. C.; Johnson, L. R.; Bliznyuk, V. N.; Schlesinger, Z.; Carter, S. A.; Horhold, H. H. *Adv. Mater.* **2000**, *12*, 1689.
(15) Koster, L. J. A.; van Strien, W. J.; Beek, W. J. E.; Blom, P. W. M. *Adv. Funct. Mater.* **2007**, *17*, 1297−1302.
(16) Beek, W. J. E.; Slooff, L. H.; Wienk, M. M.; Kroon, J. M.; Janssen, R. A. J. *Adv. Funct. Mater.* **2005**, *15*, 1703−1707.
(17) Beek, W. J. E.; Wienk, M. M.; Janssen, R. A. J. *J. Mater. Chem.* **2005**, *15*, 2985−2988.
(18) Zhang, S.; Cyr, P. W.; McDonald, S. A.; Konstantatos, G.; Sargent, E. H. *Appl. Phys. Lett.* **2005**, *87*.
(19) McDonald, S. A.; Konstantatos, G.; Zhang, S. G.; Cyr, P. W.; Klem, E. J. D.; Levina, L.; Sargent, E. H. *Nat. Mater.* **2005**, *4*, 138−U14.
(20) Cui, D. H.; Xu, J.; Zhu, T.; Paradee, G.; Ashok, S.; Gerhold, M. *Appl. Phys. Lett.* **2006**, *88*.
(21) Arici, E.; Sariciftci, N. S.; Meissner, D. *Adv. Funct. Mater.* **2003**, *13*, 165−171.
(22) Arici, E.; Hoppe, H.; Schaffler, F.; Meissner, D.; Malik, M. A.; Sariciftci, N. S. *Appl. Phys. a-Mater. Sci. Processing* **2004**, *79*, 59−64.
(23) Snaith, H. J.; Arias, A. C.; Morteani, A. C.; Silva, C.; Friend, R. H. *Nano Lett.* **2002**, *2*, 1353−1357.
(24) Huynh, W. U.; Dittmer, J. J.; Teclemariam, N.; Milliron, D. J.; Alivisatos, A. P.; Barnham, K. W. J. *Phys. Rev. B* **2003**, *67*.
(25) Schmidt-Mende, L.; Fechtenkotter, A.; Mullen, K.; Moons, E.; Friend, R. H.; MacKenzie, J. D. *Science* **2001**, *293*, 1119−1122.
(26) Gur, I.; Fromer, N. A.; Alivisatos, A. P. *J. Phys. Chem. B* **2006**, *110*, 25543−25546.
(27) Kim, S. S.; Jo, J.; Chun, C.; Hong, J. C.; Kim, D. Y. *J. Photochem. Photobiol. a-Chem.* **2007**, *188*, 364−370.
(28) Kannan, B.; Castelino, K.; Majumdar, A. *Nano Lett.* **2003**, *3*, 1729−1733.
(29) Coakley, K. M.; McGehee, M. D. *Chem. Mater.* **2004**, *16*, 4533−4542.
(30) Greene, L. E.; Law, M.; Goldberger, J.; Kim, F.; Johnson, J. C.; Zhang, Y. F.; Saykally, R. J.; Yang, P. D. *Angew. Chem.-Int. Ed.* **2003**, *42*, 3031−3034.
(31) Greene, L. E.; Law, M.; Tan, D. H.; Montano, M.; Goldberger, J.; Somorjai, G.; Yang, P. D. *Nano Lett.* **2005**, *5*, 1231−1236.
(32) Law, M.; Greene, L. E.; Johnson, J. C.; Saykally, R.; Yang, P. D. *Nat. Mater.* **2005**, *4*, 455−459.
(33) Greene, L. E.; Yuhas, B. D.; Law, M.; Zitoun, D.; Yang, P. D. *Inorg. Chem.* **2006**, *45*, 7535−7543.
(34) Olson, D. C.; Piris, J.; Collins, R. T.; Shaheen, S. E.; Ginley, D. S. *Thin Solid Films* **2006**, *496*, 26−29.
(35) Ravirajan, P.; Peiro, A. M.; Nazeeruddin, M. K.; Graetzel, M.; Bradley, D. D. C.; Durrant, J. R.; Nelson, J. *J. Phys. Chem. B* **2006**, *110*, 7635−7639.
(36) Peiro, A. M.; Ravirajan, P.; Govender, K.; Boyle, D. S.; O'Brien, P.; Bradley, D. D. C.; Nelson, J.; Durrant, J. R. *J. Mater. Chem.* **2006**, *16*, 2088−2096.
(37) Wang, H.; Oey, C. C.; Djurisic, A. B.; Xie, M. H.; Leung, Y. H.; Man, K. K. Y.; Chan, W. K.; Pandey, A.; Nunzi, J. M.; Chui, P. C. *Appl. Phys. Lett.* **2005**, *87*, 3.
(38) Coakley, K. M.; McGehee, M. D. *Appl. Phys. Lett.* **2003**, *83*, 3380−3382.
(39) Beek, W. J. E.; Wienk, M. M.; Kemerink, M.; Yang, X. N.; Janssen, R. A. J. *J. Phys. Chem. B* **2005**, *109*, 9505−9516.
(40) Xu, Y.; Schoonen, M. A. A. *Am. Mineral.* **2000**, *85*, 543−556.
(41) Quintana, M.; Edvinsson, T.; Hagfeldt, A.; Boschloo, G. *J. Phys. Chem. C* **2007**, *111*, 1035−1041.
(42) Baxter, J. B.; Schmuttenmaer, C. A. *J. Phys. Chem. B* **2006**, *110*, 25229−25239.
(43) Anderson, N. A.; Ai, X.; Lian, T. Q. *J. Phys. Chem. B* **2003**, *107*, 14414−14421.
(44) Noack, V.; Weller, H.; Eychmuller, A. *J. Phys. Chem. B* **2002**, *106*, 8514−8523.
(45) Ozgur, U.; Alivov, Y. I.; Liu, C.; Teke, A.; Reshchikov, M. A.; Dogan, S.; Avrutin, V.; Cho, S. J.; Morkoc, H. *J. Appl. Phys.* **2005**, *98*, 103.
(46) Law, M.; Greene, L. E.; Radenovic, A.; Kuykendall, T.; Liphardt, J.; Yang, P. D. *J. Phys. Chem. B* **2006**, *110*, 22652−22663.
(47) Hugger, S.; Thomann, R.; Heinzel, T.; Thurn-Albrecht, T. *Colloid Polym. Sci.* **2004**, *282*, 932−938.
(48) Sirringhaus, H. *Adv. Mater.* **2005**, *17*, 2411−2425.
(49) Sirringhaus, H.; Brown, P. J.; Friend, R. H.; Nielsen, M. M.; Bechgaard, K.; Langeveld-Voss, B. M. W.; Spiering, A. J. H.; Janssen, R. A. J.; Meijer, E. W.; Herwig, P.; de Leeuw, D. M. *Nature* **1999**, *401*, 685−688.
(50) Park, Y. D.; Cho, J. H.; Kim, D. H.; Jang, Y.; Lee, H. S.; Ihm, K.; Kang, T. H.; Cho, K. *Electrochem. Solid State Lett.* **2006**, *9*, G317−G319.
(51) Kline, R. J.; McGehee, M. D.; Kadnikova, E. N.; Liu, J. S.; Frechet, J. M. J.; Toney, M. F. *Macromolecules* **2005**, *38*, 3312−3319.
(52) Sundberg, M.; Inganas, O.; Stafstrom, S.; Gustafsson, G.; Sjogren, B. *Solid State Commun.* **1989**, *71*, 435−439.
(53) Sandberg, H. G. O.; Frey, G. L.; Shkunov, M. N.; Sirringhaus, H.; Friend, R. H.; Nielsen, M. M.; Kumpf, C. *Langmuir* **2002**, *18*, 10176−10182.
(54) Olson, D. C.; Lee, J. Y.; White, M. S.; Kopidakis, N.; Shaheen, S. E.; Ginley, D. S.; Voigt, J. A.; Hsu, J. W. P. *J. Phys. Chem. C* **2007**, *111*, 16640−16645.
(55) Olson, D. C.; Shaheen, S. E.; White, M. S.; Mitchell, W. J.; van Hest, M.; Collins, R. T.; Ginley, D. S. *Adv. Funct. Mater.* **2007**, *17*, 264−269.
(56) Lira-Cantu, M.; Norrman, K.; Andreasen, J. W.; Casan-Pastor, N.; Krebs, F. C. *J. Electrochem. Soc.* **2007**, *154*, B508−B513.
(57) Lira-Cantu, M.; Norrman, K.; Andreasen, J. W.; Krebs, F. C. *Chem. Mater.* **2006**, *18*, 5684−5690.
(58) Brajsa, A.; Szaniawska, K.; Barczynski, R. J.; Murawski, L.; Koscielska, B.; Vomvas, A.; Pomoni, K. *Opt. Mater.* **2004**, *26*, 151−153.
(59) Eppler, A. A.; Ballard, I. N.; Nelson, J. *Phys. E-Low-Dimensional Syst. Nanostruct.* **2002**, *14*, 197−202.
(60) Wahlstrom, E.; Vestergaard, E. K.; Schaub, R.; Ronnau, A.; Vestergaard, M.; Laegsgaard, E.; Stensgaard, I.; Besenbacher, F. *Science* **2004**, *303*, 511−513.
(61) Xiao-e, L.; Green, A. N. M.; Haque, S. A.; Mills, A.; Durrant, J. R. *J. Photochem. Photobiol. a-Chem.* **2004**, *162*, 253−259.